Carbohydrate Polymers 97 (2013) 458–468

Contents lists available at SciVerse ScienceDirect

Carbohydrate Polymers

journal homepage: www.elsevier.com/locate/carbpol

Structural variability between starch granules in wild type and in *ae* high-amylose mutant maize kernels

Dongli Liu[a], Mary L. Parker[b], Nikolaus Wellner[b], Andrew R. Kirby[b], Kathryn Cross[b], Victor J. Morris[b], Fang Cheng[a,*]

[a] College of Biosystems Engineering and Food Science, Hangzhou, Zhejiang University, 310058 PR China
[b] Institute of Food Research, Norwich Research Park, Norwich NR4 7UA, UK

ARTICLE INFO

Article history:
Received 28 January 2013
Received in revised form 7 April 2013
Accepted 9 May 2013
Available online 15 May 2013

Keywords:
High-amylose maize
ae maize
Electron microscopy
Atomic force microscopy
Light microscopy
Raman spectroscopy
Infra-red spectroscopy
Kernel structure

ABSTRACT

Starch granule structure within wild-type and *ae* high-amylose mutant maize kernels has been mapped *in situ* using light, electron and atomic force microscopy, and both Raman and infra-red spectroscopy. The population of wild-type starch granules is found to be homogenous. The *ae* mutant granule population is heterogeneous. Heterogeneity in chemical and physical structure is observed within individual granules, between granules within cells, and spatially within the kernel. The highest level of heterogeneity is observed in the region where starch is first deposited during kernel development. Light microscopy demonstrates structural diversity through use of potassium iodide/iodine staining and polarised microscopy. Electron and atomic force microscopy, and infra-red and Raman spectroscopy defined the nature of the structural changes within granules. The methodology provides novel information on the changes in starch structure resulting from kernel development.

1. Introduction

Knowledge of the structure of starch is important for understanding functionality and considerable progress has been made over the last 30 years in understanding the nature of the internal structure of starch granules (Pérez & Bertoft, 2010). Wild-type (WT) starch granules are homogeneous structures and the properties of individual granules can be deduced from studies on populations of isolated granules. The current view of the internal structure of starch granules has been largely derived from microscopy and scattering studies (Pérez & Bertoft, 2010).

Key results of these investigations include the following observations. Conventional light microscopy has revealed spheroidal structures of various size and shape, dependent on source (Pérez & Bertoft, 2010). Differential interference contrast and confocal microscopy, together with various staining methods, have revealed the existence of periodic growth ring structures within hydrated granules (Blennow et al., 2003; Gallant, Bouchet, & Baldwin, 1997; Pérez & Bertoft, 2010; van de Velde, van Riel, & Tromp, 2002). X-ray diffraction studies demonstrate that the granules are semi-crystalline, with the type of crystal structure dependent on source (Pérez & Bertoft, 2010). Observation of the granules between crossed polarisers reveals characteristic 'Maltese cross' patterns that demonstrate the radial orientation of ordered (crystalline) structures within the granules (Gallant et al., 1997; Pérez & Bertoft, 2010). High-resolution transmission electron microscopy (TEM) has shown the existence of the basic underlying structural units (platelet nanocrystals) within the granule (Gallant et al., 1997). Early microscopy studies on chemically-etched and enzymatically-degraded granules showed the loss of alternate growth rings. The cluster model of starch ultrastructure, deduced from the modelling of largely small-angle X-ray scattering (SAXS) and small-angle neutron scattering (SANS) data (Blazek & Gilbert, 2011; Cameron & Donald, 1992; Daniels & Donald, 2003, 2004; Donald, Kato, Perry, & Waigh, 2001; Waigh, Perry, Rickel, Gidley, & Donald, 1998; Waigh et al., 2000) is thus based on a granule composed of alternating amorphous and crystalline growth rings, with the crystalline rings containing bundles (blocklets) of interconnected crystal lamellae. These scattering studies have been refined to describe the crystalline structures within the granule. Although the crystalline regions within the granules are well-defined, more recent TEM and atomic force microscopy (AFM) studies show an absence of amorphous growth rings, revealing a continuous semi-crystalline structure throughout the granule, with the blocklets embedded

* Corresponding author. Tel.: +86 571 88982713; fax: +86 571 88982713.
E-mail address: fcheng@zju.edu.cn (F. Cheng).

0144-8617/$ – see front matter © 2013 Elsevier Ltd. All rights reserved.
http://dx.doi.org/10.1016/j.carbpol.2013.05.013

in an amorphous matrix (Gallant et al., 1997; Morris, Ridout, & Parker, 2005; Parker, Kirby, & Morris, 2008; Ridout, Gunning, Wilson, Parker, & Morris, 2002; Ridout, Parker, Hedley, Bogracheva, & Morris, 2004). The growth ring structure appears to arise from selective swelling of alternating semi-crystalline growth rings with different amorphous-crystalline ratios.

Gelatinisation of starch releases two polysaccharides, amylose and amylopectin. Amylopectin is a highly-branched molecule that is considered to arise from the crystalline structures (blocklets) within the granule: the branches of the amylopectin molecules are present in the granule as the radially-orientated crystalline lamellae within the blocklets. Amylose is an essentially linear molecule, considered to arise from the amorphous regions within the starch granule. Nowadays there is a growing interest in measuring and defining the changes in granule structure that result from selected mutations in starch biosynthesis. Natural or induced mutations lead to 'low-amylose' and 'high-amylose' starches, although in fact, particularly for the high-amylose starches, these mutations lead to a range of molecular structures released from the granule on gelatinisation including, as well as amylose and amylopectin, an intermediate material variously called more-highly-branched amylose or a modified amylopectin (Pérez & Bertoft, 2010). Despite their nomenclature it is clear that such mutations actually lead to significant modifications of the starch granule structure rather than simply altering the levels of amylose and amylopectin that can be isolated from the granules. Even in the case of isogenic mutants such as *amylose extender ae* (high-amylose) maize, studies on individual granules reveal heterogeneity in structure within populations of isolated starch granules (Chen, Yu, Chen, & Li, 2006; Evans, McNish, & Thompson, 2003; Katz, Furesik, Tenbarge, Hauber, & Friedman, 1993). To understand how these mutations in biosynthesis determine the resultant granule structures, it is useful to map the chemical and physical structures of individual granules directly within seeds. The spatial distribution of granule structure provides information on the changes in granule structure during development of the seeds. Populations of isolated starches from the single *ae* mutant maize contain a small percentage (~1.7%) of elongated compound granules, not observed in WT maize. The GEMS-0067 mutant (Campbell, Jane, Pollak, Blanco, & O'Brien, 2007) which contains a high amylose moderator gene (HAM), has a higher 'amylose' content (~81–86%) than the single *ae* mutant (~61–68%) (Li, Jiang, Campbell, Blanco, & Jane, 2008), or the WT starch (~30%) (Hasjim, Srichuwong, Scott, & Jane, 2009). The starch isolated from mature GEMS-0067 seeds contains a higher percentage (~32%) of elongated granules (Jiang, Horner, et al., 2010). Developmental studies (Jiang, Lio, Blanco, Campbell, & Lane, 2010) suggest that the percentage of these elongational structures increases with maturity and that their presence is related to an increased resistant starch (RS) content.

The present studies on the single *ae* mutant are designed to characterise the distribution of granule structures directly within seeds. They build on previous *in situ* imaging of starch in dry seeds (Matsushima, Maekawa, Fujita, & Sakamoro, 2010; Parker et al., 2008; Wellner, Georget, Parker, & Morris, 2011). Low resolution 2D and reconstructed 3D images of wild-type and high-amylose rice kernels, using X-ray microtomography and environmental SEM, have been reported recently by Zhu and co-workers (Zhu et al., 2012). Higher resolution studies on starch granule structures in WT and *ae* mutant maize kernels, using iodine staining, polarised light microscopy and Raman microscopy revealed the heterogeneity within the kernel (Wellner et al., 2011) responsible for that observed for isolated starches (Chen et al., 2006; Evans et al., 2003; Katz et al., 1993). These studies identified the physical and chemical origins of this heterogeneity through high-resolution chemical mapping of the structure of individual granules. This article describes the use of iodine staining and polarised light microscopy to map variations in structural heterogeneity for WT and *ae* maize starch granules spatially within kernels, and the use of TEM, scanning electron microscopy (SEM), and AFM to probe the structural basis of the heterogeneity.

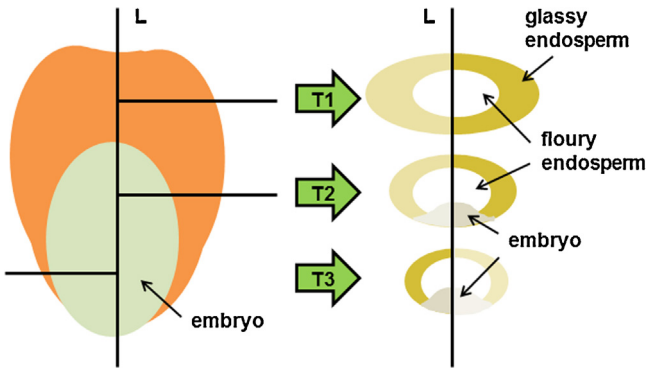

Fig. 1. Preparation of dry-cut sections and endosperm blocks from WT and *ae* maize kernels. (a) *ae* maize kernel. (b) Sampling positions for transverse sections T1-4, and for longitudinal section *L*.

2. Materials and methods

2.1. Maize kernel sections

Kernels of wild-type (WT) maize (cultivated Oh 43) and the high-amylose *amylose extender* (*ae*) mutant in an Oh 43 background were kindly provided by Dr K. Denyer (John Innes Centre, Norwich, UK) and Professor C Weil, (Department of Agronomy, Purdue University, West Lafayette, USA). The seeds used in the study are mature seeds.

To compare the spatial variability within WT and mutant maize kernels, thin sections were cut directly from four locations in the grain. Each kernel was first cut in two halves along the long axis *L* (Fig. 1) using a fine-toothed saw. Then the halves were clamped in the specimen holder of an ultra-microtome (Reichert-Jung Ultracut E) and positioned so that transverse cuts could be made from three different positions in the kernel, just below the crown (T1), mid-kernel (T2), and the lower part of the kernel (T3), as shown in the schematic diagram (Fig. 1). Longitudinal sections were also cut from the position *L*. At each position, the bulk of the overlying endosperm was first removed with the fine-toothed saw, taking care not to overheat the adjacent endosperm. Then the rough surface was planed away with a glass knife until a polished mirror-like surface was obtained. Consecutive dry-cut sections of endosperm tissue, nominally 1.5–2 μm thick, could then be cut directly from this flat surface to include bran layers, aleurone layer, outer vitreous endosperm and inner floury endosperm, and also embryo tissue in *L*, T2 and T3. Sometimes, cutting of sections led to loss of the embryo and part of the floury region of the endosperm. Sections could be imaged by light microscopy or atomic force microscopy (AFM), and AFM and SEM could also be used to image directly the polished surfaces. Because all the sections were cut sequentially from each sampling position they were almost identical and the results obtained using the different measurement techniques could be compared.

2.2. Light microscopy

Sections were transferred to a small drop of distilled water on a glass microscope slide, the excess water was quickly drained off and the sections were allowed to dry in an oven at 30 °C. The sections were stained with 0.2% iodine in 2% potassium iodide diluted 2:1 with distilled water (KI/I_2) then viewed and photographed in bright

field using an Olympus BX60 light microscope (Olympus, Japan) with ProgRes® Capture Pro 2.1 software (Jenoptik, Germany). For polarised light microscopy, sections dried onto slides were examined unstained using the polarising optics of the microscope.

2.3. Electron microscopy

2.3.1. Scanning electron microscopy

Blocks of endosperm tissue, each with a surface polished as in Section 2.1 were mounted, polished surface uppermost, on aluminium stubs using silver-conducting paint. Some blocks were then gold coated in an Agar high-resolution sputter-coater, other blocks were first passed briefly through steam to humidify the polished surface, and then allowed to dry at room temperature before coating. To produce a fracture surface rather than a cut surface of the endosperm cell contents, a shallow slot was first sawn into the kernel in the plane *L*. A dull blade was inserted into the slot with sufficient pressure to split the kernel into two. The endosperm halves were mounted on stubs and coated with gold. All samples were examined and photographed in a Zeiss Supra 55 VP FEG SEM, operating at 3 kV.

2.3.2. Transmission electron microscopy

Mature kernels of *ae* maize were imbibed between wet filter paper in a petri dish at 4 °C overnight. Small cubes of tissue, approx. 1 mm^3, were cut from the inner endosperm at position T1 at the crown of the kernel and fixed in 3% glutaraldehyde (Agar Scientific, Stansted, UK) in 0.1 M cacodylate buffer (pH 7.2) for approximately 4 h. The tissue pieces were post-fixed in 1% aqueous osmium tetroxide overnight, then dehydrated through an ethanol series and infiltrated in LR White medium grade resin (London Resin Company Ltd.). The samples were polymerised in gelatin capsules at 60 °C overnight. Sections approximately 90 nm thick were cut with a diamond knife using an ultramicrotome (Ultracut E, Reichert-Jung). Sections collected on copper grids were stained sequentially with uranyl acetate (saturated in 50% ethanol) and Reynold's lead citrate. Sections were examined and imaged in a FEI Tecnai G2 20 Twin transmission electron microscope at 200 kV.

2.4. Atomic force microscopy

Studies were made on sections dried onto glass slides, as described in a previous publication (Parker et al., 2008), and on dry or humidified polished blocks.

The instrument used in these experiments was an MFP-3D Bio (Asylum Research, Santa Barbara, CA). It was principally operated in Tapping mode in air using AC160TS cantilevers (Olympus, Japan). Typical resonant frequencies for these cantilevers were ~300 kHz, and their spring constant ~43 Nm^{-1}. Owing to the relatively rough nature of the samples it was important to scan at low rates, particularly when imaging larger areas (>10 μm). Scan rates employed in these experiments were in the range 0.3–0.5 Hz. The scan angle was set to 90° for all but the smallest scans (<2 μm) where it was returned to 0°. This is beneficial because it reduces the incidence of skipping and mistracking for larger scans, although the sensitivity is reduced slightly (Kirby, 2011).

2.5. FTIR and Raman spectroscopy

1–2 μm thick WT and *ae* sections were transferred to a small drop of distilled water onto BaF_2 disks (13 mm diameter, 1 mm thick), the excess water was quickly drained off and the sections were allowed to dry.

FT-IR data were acquired with a Varian UMA600 microscope interfaced to a FTS6000 FT-IR spectrometer (Digilab/Varian). Average spectra were collected in transmission mode from a 1 mm diameter sample spot with a MCT detector. 128 scans at a resolution of 2 cm^{-1} were averaged and referenced against a background from an empty area of the BaF_2 disc. The spectra were baseline-corrected in the region (1800–900 cm^{-1}) and Fourier-deconvoluted using a 10 cm^{-1} bandwidth and an enhancement factor of 2.0. Raman data were obtained using an upgraded WITec CRM200 (Witec GmbH, Ulm, Germany) confocal microscope using a frequency-doubled Nd YAG laser (532 nm) and a ×100 objective. Raman spectra were collected in backscattering mode using a 600 nm grating in the spectral range −30 to 3980 cm^{-1}. Raman spectra were baseline-corrected by subtraction of the value at 1800 cm^{-1} as a linear offset.

3. Results and discussion

3.1. Optical microscopy of the WT and ae mutant

The optical microscopy studies revealed marked differences between the internal structure of the WT and *ae* mutant starches. Dry-cut sections of kernels examined by KI/I_2 staining and polarising microscopy, showed that the WT starch granules are homogeneous within the kernel: they stain uniformly blue with KI/I_2 in all endosperm cells at positions TI (Fig. 2a), T2 and T3 and show characteristic Maltese cross patterns, indicating radial orientation of the crystalline regions within the granules (Fig. 2b). At higher magnification, the granules reveal growth ring structures indicating a periodic radial variation in the crystalline/amorphous ratio within the granule. The data shown is representative of observations made on dozens of seeds.

For the *ae* mutant, optical microscopy of transverse dry-cut sections from position T1 (Fig. 3a) and from just below the crown of longitudinal sections from position *L* (Fig. 3b) reveals gross heterogeneity in the way the starch granules stain with KI/I_2. At position T1, there is a narrow band of sub-aleurone endosperm cells with predominantly blue-staining granules, and a central endosperm region with predominantly pink-staining granules. Studies of sections cut from T1-3 show heterogeneity in staining within individual granules, between granules within cells, and between cells across the kernel. Fig. 4a–f shows representative regions of KI/I_2 stained sections from the outer and inner regions of *ae* endosperm at these positions T1-3 indicated in Fig. 1. The data show that the major heterogeneity occurs in the sections from T1: this is the region investigated in the previous study on starch structure in *ae* mutant kernels (Wellner et al., 2011). As described previously, the spheroidal starch granules of the outer endosperm of *ae* tend to be smaller than those in the WT, with evidence for the presence of elongated and dimpled granules (Chen et al., 2006; Evans et al., 2003; Jiang, Horner, et al., 2010; Jiang, Lio, et al., 2010; Katz et al., 1993) on isolated *ae* mutant starch. In the outer endosperm at position T1, the majority of the granules stain blue with KI/I_2 (Fig. 4a), with only occasional biphasic granules showing a central region that stains blue, and an outer region of variable thickness that stains pink. The inner endosperm at T1 exhibits the widest variation between blue- and pink-stained granules with pink-stained material at the periphery of the granules (Fig. 4b): the central hilum cavity of the blue regions enlarges when the starch granule swells in the aqueous mounting conditions and remains unstained. The level of heterogeneity in the T1 endosperm can vary markedly at boundaries between neighbouring cells and, in general, tends to become more heterogeneous as sampling progresses from the outer to the inner endosperm. The population of granules is very diverse, ranging from granules that stain blue in colour, through a range of biphasic granules containing blue- and pink-stained regions, to granules that are largely pink in colour. Within position T2 the variation across the endosperm is less pronounced but there are proportionally more

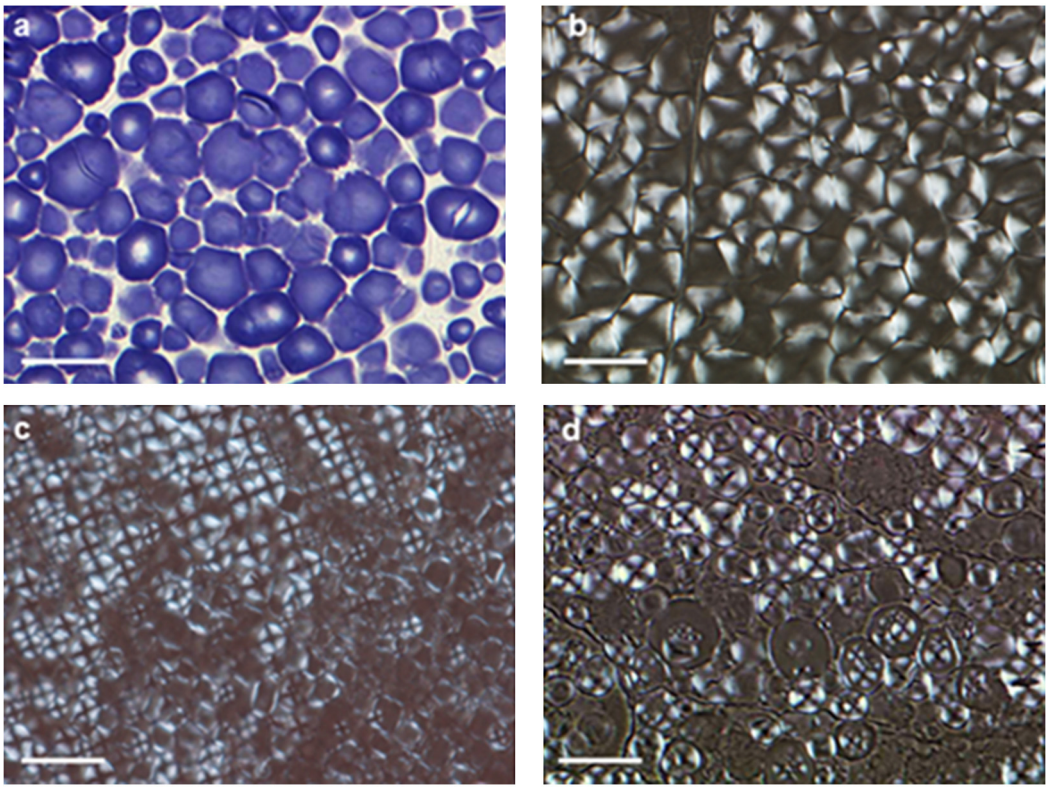

Fig. 2. KI/I_2 staining and polarised microscopy of dry-cut sections of maize kernels. Bar markers are 20 μm. (a) WT starch stained with KI/I_2 is uniformly blue throughout the endosperm. (b) WT starch viewed by polarised microscopy show Maltese crosses. (c and d) Starch granules from the central region of *ae* endosperm at position T1 viewed by polarised microscopy exhibit heterogeneity in the distribution and size of Maltese crosses with some granules and some regions of granules showing no Maltese crosses. (For interpretation of the references to color in this figure legend, the reader is referred to the web version of this article.)

granules containing pink regions in the inner endosperm (Fig. 4c and d). At position T3 (Fig. 4e and f) the variation is even less pronounced, with very few granules containing pink-staining regions (Fig. 4f). Thus the greatest level of heterogeneity occurs in the inner region of the endosperm, just below the crown of the kernel, and becomes progressively less towards the base of the kernel. This would suggest that the greatest level of heterogeneity arises in starch granules that are laid down early in the growth of the seed, and that the level of heterogeneity is less in granules deposited later during subsequent development of the kernel. These observations were typical of studies made on dozens of seeds of this particular line. The data shown in Figs. 3 and 4 suggest that KI/I_2 staining on dry-cut sections provides an easy screening test for structural heterogeneity and allows the location of these structural variations to be mapped within the kernel.

Polarised light microscopy of the outer and inner *ae* endosperm also emphasised the same variations in structural heterogeneity (Fig. 2c and d). As with the KI/I_2 staining, the greatest level of structural heterogeneity is observed in the inner endosperm of sections from T1 and the heterogeneity becomes less pronounced at T2 and then T3. The polarised microscopy provides additional information on the alignment of the ordered (crystalline) structure within the pink- and blue-staining areas of the granules. The images in the most structurally-heterogeneous part of sections from T1 (Fig. 2c and d) reveal surprising and unexpected features: some granules show ordered (crystalline) structures that

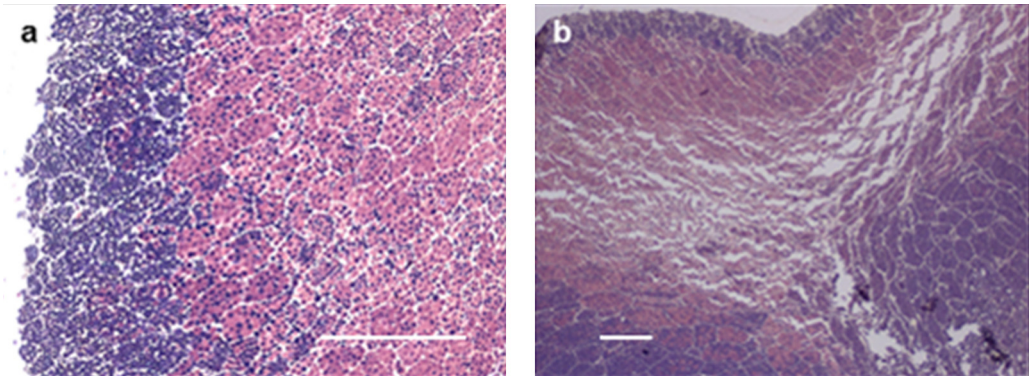

Fig. 3. Low magnification images of sections of *ae* kernels. (a) KI/I_2 stained dry-cut section from position T1 showing (left) the narrow band of sub-aleurone endosperm cells containing predominantly blue-staining granules. In the central endosperm (right), just below the crown of the kernel, the starch granules are predominantly pink-staining. Bar marker is 200 μm. (b) KI/I_2 stained longitudinal section (*L*) showing the central location of predominantly pink-staining granules at the crown of the kernel. Bar marker is 200 μm. (For interpretation of the references to color in this figure legend, the reader is referred to the web version of this article.)

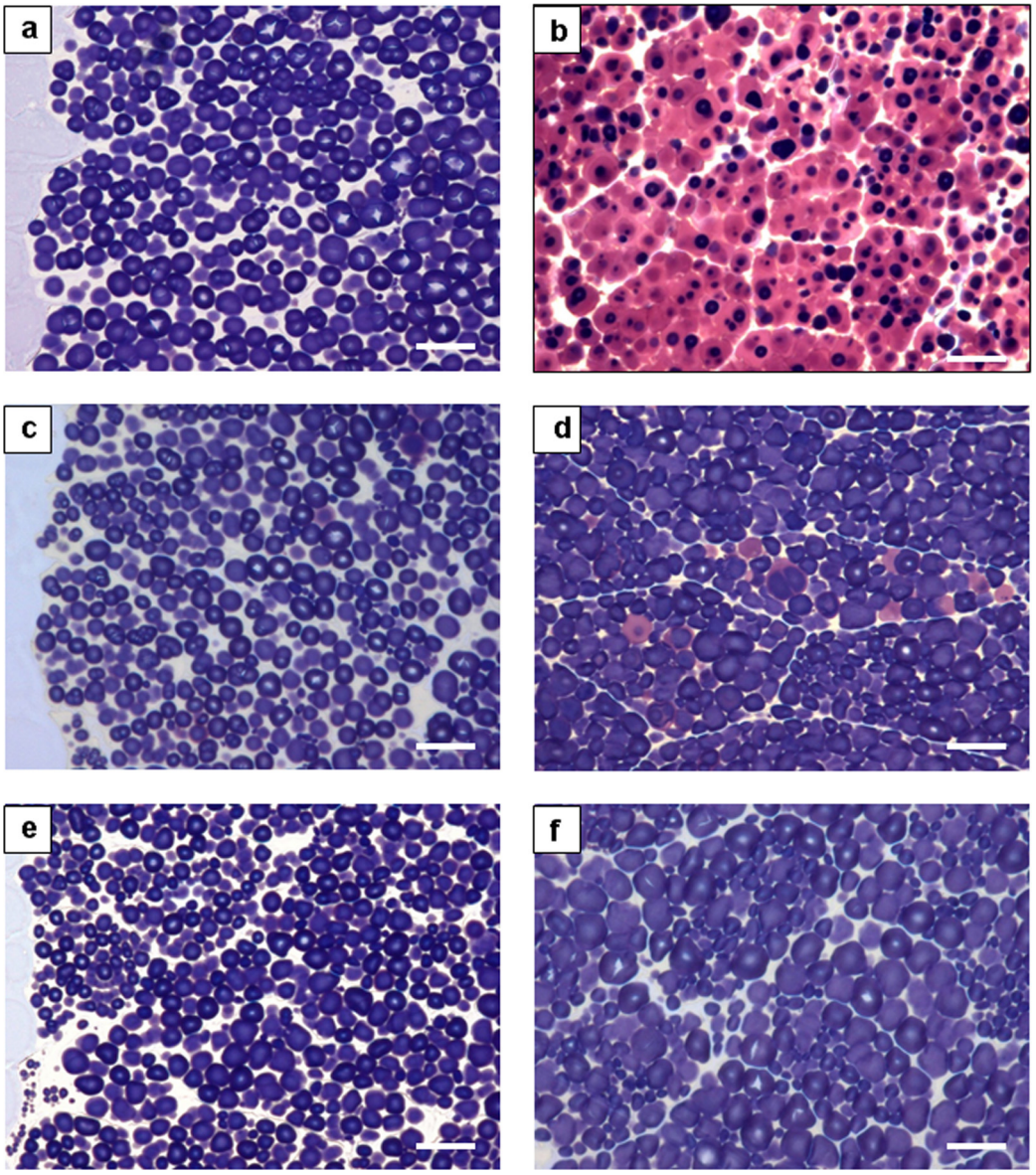

Fig. 4. KI/I_2 stained dry-cut sections from *ae* kernels. Bar markers are 20 μm. (a) T1 outer endosperm. (b) T1 inner endosperm with extensive pink-staining granules. (c) T2 outer endosperm. (d) T2 inner endosperm with some pink-staining granules. (e) T3 outer endosperm. (f) T3 inner endosperm. (For interpretation of the references to color in this figure legend, the reader is referred to the web version of this article.)

are radially-aligned and homogeneous, some granules show no radial alignment, and other granules show various intermediate structures containing one or more radially-aligned regions within the granules, and a peripheral region with no radial alignment (Fig. 2c and d). In general the blue-staining regions are those that show characteristic, conventional 'Maltese cross' patterns, whilst the pink-staining areas show no evidence of radial alignment of the molecular structure. The presence of granules showing several areas within the granule where the molecular structure is aligned, existing within a background of unaligned material, plus the presence of apparently normal, blue–staining granules, and grossly abnormal, pink-staining granules is most surprising and difficult to explain: isolated *ae* single mutant starch granules normally stain blue with iodine when viewed under bright field microscopy (Evans et al., 2003; Seckinger & Wolf, 1966) and show only a small percentage of complex 'compound' granules (Jiang, Horner, et al., 2010). These images clearly show that a single mutation in an isogenic line does not result in a simple change in the ratio of amylose and amylopectin within the granules, but rather complex and variable granule structures resulting from development of the kernel.

For the *ae* mutant the data shown is representative of studies on dozens of seeds. The starch granules within a particular seed are hetereogeneous, and the structure of individual granules within a population varies from one seed to another. However, the general and common observation is that the most severe level of structural diversity is located at a central region within the inner endosperm of the kernel and becomes less pronounced as the extremities of the kernel are approached. The images shown were selected to illustrate the structural heterogeneity within granules and its variation within the kernel.

3.2. FTIR and Raman spectroscopy of the WT and ae mutant

FTIR and Raman spectra were used to compare the chemical composition and structure of the WT and the *ae* mutant maize. The FTIR spectra show strong absorption in both the protein and carbohydrate regions. The carbohydrate region is dominated by starch,

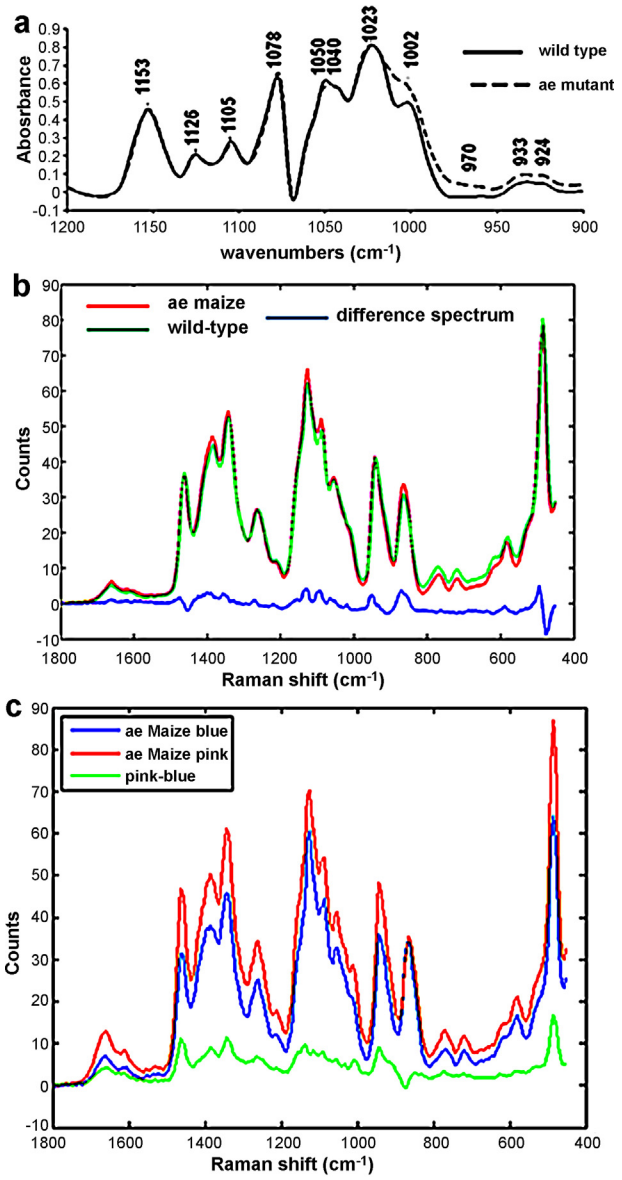

Fig. 5. FTIR and Raman spectra. (a) Comparison of FTIR spectra for WT and *ae* maize sections. (b) Comparative Raman spectra for WT and *ae* sections and the difference spectrum. (c) Comparative Raman spectra for representative blue- and pink-staining regions of *ae* mutant starch granules and the difference (pink–blue) spectrum. (For interpretation of the references to color in this figure legend, the reader is referred to the web version of this article.)

with only a minor contribution from non-starch cell-wall components. WT and *ae* mutant FTIR spectra show similar amide I bands at 1650 cm^{-1}, indicating a comparable level of protein content. However, there were consistent differences in the starch bands, particularly in the region of the absorption spectrum sensitive to the crystal structure of the starch (Fig. 5a). Fourier-deconvolution of the carbohydrate region resolved bands at 1153, 1126, 1105, 1078, 1050, 1044, 1023, 1002, 933 and 924 cm^{-1} The *ae* maize spectra showed a larger 1002 cm^{-1} band and also some broadening, resulting in greater overlap with the main 1023 cm^{-1} band and some absorption around 970 cm^{-1}. The band at 1050 cm^{-1} was found to be slightly smaller than the equivalent band for the WT samples. Amorphous starch shows a peak at 1022 cm^{-1} whereas lintnerised and granular starches are characterised by a band at 1000 cm^{-1}. The ratio of these two bands is affected by water content and indicates a change in the short-range order of amylosic helices within the crystal structure (Capron, Robert, Colonna, Brogly, & Planchot, 2007), because the 1047 cm^{-1} band, which has also been linked to starch crystallinity (vanSoest, Tournois, deWit, & Vliegenthart, 1995), is slightly lower in the *ae* maize samples. These differences in the two bands at 1047 and 1002 cm^{-1} suggest that the starch structure in the *ae* maize mutant is significantly different from that of the WT. These data are consistent with well-documented observations from X-ray diffraction that the *ae* mutation leads to a progressive transition from A- towards B-type crystals. High-resolution Raman microscopy has recently been used to study the starch structure within individual granules (Wellner et al., 2011). Fig. 5 also shows comparative Raman spectra for the WT and *ae* starch (Fig. 5b), and for representative blue- and pink-staining regions of *ae* mutant starch granules (Fig. 5c).

The maps of the ratio of the 865 cm^{-1} and 942 cm^{-1} Raman bands exhibited dichroic effects (Wellner et al., 2011), indicative of the orientation of ordered (crystalline) structures within the granules, and equivalent to the Maltese cross patterns obtained by conventional polarised light microscopy (Fig. 2b). These data confirmed that the WT granule structures are homogeneous and the crystalline structures are radially orientated. In the *ae* maize sections, the Raman maps (Wellner et al., 2011) showed heterogeneity equivalent to that observed by polarised light microscopy and KI/I_2 staining. Notably, evidence for radial alignment was only found in the blue-staining region of the granules. As reported previously, the ratio of the bands at 952 cm^{-1} and 942 cm^{-1} is sensitive to the ratio of linear/branched residues (Liu, Himmelsbach, & Barton, 2004). The *ae* mutation results from the suppression of the activity of the starch branching enzyme IIb (SBEIIb) and, as expected, the Raman spectra for the *ae* mutant starches show a higher band at 952 cm^{-1} from unbranched starch when compared to the WT (Fig. 5b). The Raman spectra shown in Fig. 5c give evidence for a smaller, but detectable reduction in the level of branching in the pink-staining regions, when compared to the blue-staining region of the biphasic granules. Finally the 486 cm^{-1}/942 cm^{-1} band ratio is sensitive to order (crystallinity): the maps of this ratio revealed that the WT starch granules are homogeneous and that the overall level of crystallinity in the *ae* mutant was lower than in the WT. For individual granules, the maps reported previously (Wellner et al., 2011) and the spectra shown in Fig. 5c demonstrate that the level of order (crystallinity) in the outer pink-staining regions of the granules appears slightly more ordered (crystalline) than the central blue-staining regions, and less than in the WT starch. These data show that the KI/I_2 staining pattern not only maps changes in chemical composition, but also molecular alignment and ordering resulting from the *ae* mutation, and allows characterisation of the localised heterogeneity within individual granules.

Clearly in a proportion of the granules within the kernel the *ae* mutation results in the presence of two regions separated by a distinct boundary. Electron microscopy and AFM provide methods for visualising the ultrastructure within granules and thus should reveal differences in structure within the WT starch, and for the pink- and blue-staining regions within the *ae* mutant starch granules.

The following images are not intended to be a comprehensive study using SEM, AFM and TEM, but rather to illustrate the pertinent features that can be obtained using these methods to characterise the WT and mutant starch samples, and to indicate how these techniques could be extended to characterise further the structural changes within the granules.

3.3. Scanning electron microscopy of WT and ae mutants

Fig. 6a shows an FEG-SEM image from position T1 of a polished surface of non-humidified WT endosperm. The outline of individual starch granules can be identified and there are a number of

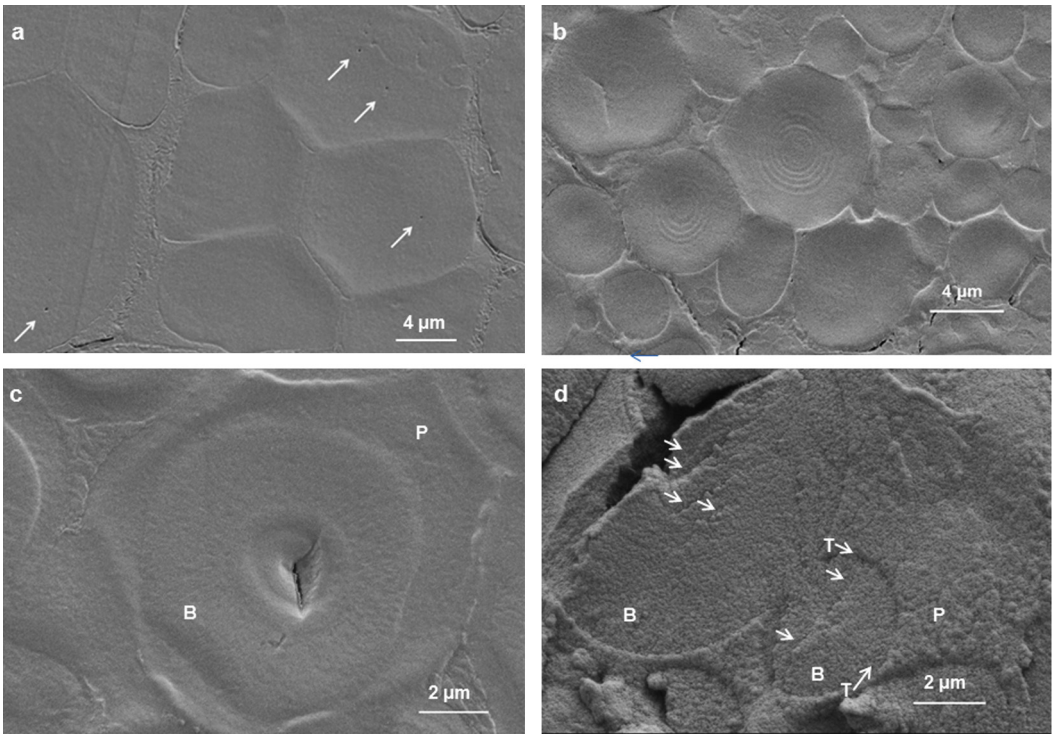

Fig. 6. FEG-SEM images of polished endosperm blocks from T1. (a) Outlines of starch granules are visible in non-humidified WT endosperm. Holes (arrowed) are characteristic of channels in WT starch. (b) Individual biphasic *ae* starch granules after sufficient hydration to reveal the growth ring structure within the central (blue-staining) regions of the granules. (c) Differential swelling of the blue- (B) and pink- (P) staining regions within the *ae* granules in a humidified block. (d) Fracture surface of biphasic *ae* granules split open almost at mid-point and showing the distinct pink (P) and blue (B) internal regions. The fractures reveal layering (arrowed) of the blocklet structure and a clearly-defined transition region (T) between pink- and blue-staining regions. (For interpretation of the references to color in this figure legend, the reader is referred to the web version of this article.)

visible holes (arrowed), which are characteristic of the channels within starch granules from sub-aleurone maize endosperm. Otherwise, within dry samples there is little evidence of internal starch structure. Previously it has been shown that selective absorption of water at the cut surface of starch leads to differential swelling (Morris et al., 2005; Parker et al., 2008) and that these height differences can reveal the growth ring structure within the granule. Fig. 6b shows FEG-SEM images of biphasic starch granules of *ae* maize from position T1 after sufficient hydration to reveal the growth rings at the centre of the granules, identifying these rings with the blue-staining regions shown in Figs. 3 and 4. No holes were observed in these hydrated samples: either channels are absent in biphasic granules, or hydration and swelling may have obscured them. The appearance of growth rings in the central region of these granules implies differential swelling of these regions and indicates differences in ultrastructure between the blue- and pink-staining regions. This is consistent with the polarised light microscopy data shown in Fig. 2 and previously reported Raman microscopy data (Wellner et al., 2011). Not all the granules appear to be hydrated to the same extent and Fig. 6c shows a higher magnification image through a biphasic *ae* granule where the inner blue region (B) appears as a raised dome-like structure, again indicating differential swelling of the blue- and pink-staining (P) regions within the granules. In previous studies on starch granules (Parker et al., 2008) it was not possible to resolve the underlying blocklet structure using a conventional SEM. However, the use of FEG-SEM reveals some underlying ultrastructure that can be seen in images of fractured samples (Fig. 6d). The image in Fig. 6d shows a biphasic *ae* granule fractured almost across its mid-point and clearly displaying the two distinct internal regions (B and P). Fracturing, rather than cutting, reveals the presence of layered structures (arrowed) containing spheroidal features identified as blocklet structures. The images suggest compact continuous arrays of these blocklets throughout the blue-staining (B) parts of the granule. Blocklet-like structures are seen in the outer pink-staining (P) regions too, but there the size of the blocklets and level of organisation is less regular. There are clear boundaries between the blue- and pink-staining areas but the nature of the transition region (arrowed and marked T) is unclear. Thus the blue- and pink-staining reflects genuine structural changes at the ultrastructural (blocklet) level within the granule. These structural changes should also be visible by AFM.

3.4. AFM studies of WT and ae maize mutants

Fig. 7a shows a high-resolution AFM topographical image of part of the growth ring structure (arrowed) within a WT starch granule imaged *in situ* at the surface of a block of humidified polished endosperm from T1. As observed previously in images of pea starch granules (Parker et al., 2008), the growth ring structure arises from patches with a higher crystalline/amorphous ratio in alternate growth rings, which show restricted swelling on hydration. The image shown in Fig. 7a shows the underlying blocklet structure within the growth rings. In the previous study on pea starch (Parker et al., 2008), a comparison of topographic and phase images revealed that the blocklet structure was regular and continuous within the granule. It has been shown (Parker et al., 2008) that the growth rings become visible when there is selective hydration of the sample: the regions that preferentially absorb water swell and become softer. Whereas the SEM sees only the changes in height, both factors contribute to contrast in the AFM topographical images. Fig. 7b shows an error signal mode (force) AFM image of a biphasic *ae* starch granule in region T1 of similarly-humidified polished block, where the growth-ring structures are visible, again only in the central blue-staining region

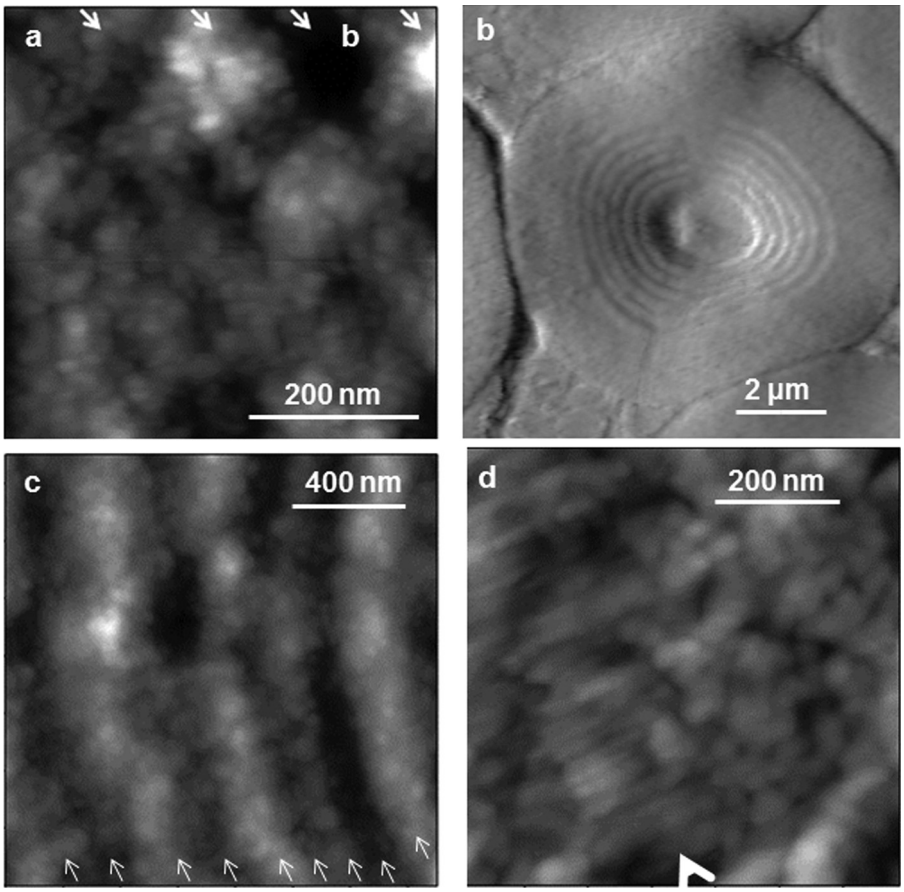

Fig. 7. AFM images of polished and humidified endosperm blocks from T1. (a) High resolution topographical image of part of the growth ring structure within a WT starch granule. Individual growth rings are arrowed. (b) Error signal mode image of a biphasic *ae* granule showing the growth rings confined to the central blue-staining region. (c) Higher-resolution topographical image of the blocklet structure within the growth rings in a biphasic *ae* granule. Individual growth rings are arrowed. (d) High-resolution topographical image of the transition region (arrowed) between blue- and pink-staining regions. (For interpretation of the references to color in this figure legend, the reader is referred to the web version of this article.)

of the granule: the wetting increases the roughness of the surface and the detail is more easily seen in the error signal mode image than in the topographical image (not shown). Higher-resolution topographical AFM images of the growth rings (Fig. 7c, arrowed) reveal the underlying blocklet structure within the granules. As observed for starch in WT maize, the growth rings arise due to isolated regions within the granule that show restricted swelling. In the present study, the sizes of the blocklets observed by FEG-SEM (Fig. 6b) and AFM (Fig. 7c) are comparable: the close packing of blocklets eliminates probe-broadening effects allowing the dimension observed in the AFM images to be compared directly with those observed in the FEG-SEM images. Typically the major blocklet dimensions are ~40–60 nm. Fig. 7d shows the transition region between the blue- and pink-staining regions of a biphasic granule, revealing a line of radially-aligned, elongated structures (arrowed) at the interface of the blue- and pink-staining regions. Thus both SEM and AFM reveal different ultrastructure in the blue- and pink-staining regions of the biphasic starch granules, and the AFM images provide additional information on the structure within the boundary region between these two areas.

3.5. TEM images of starch granules in ae mutant seeds

Finally, Fig. 8a shows TEM sections of biphasic starch granules cut from position T1 of an *ae* mutant maize kernel. The image confirms the existence of radially-aligned elongated structures (arrowed) at the boundary between the blue- (B) and pink- (P) staining regions. These are seen more clearly in the higher-magnification image in Fig. 8b. Despite the different contrast mechanisms, and the different sample preparations, the three techniques reveal similar structures for these biphasic starch granules. The fibrous protrusions from the growing surface of the blue-staining regions reveal the progressive loss of the radially-aligned structure, leading to the unoriented, but ordered structures in the pink-staining regions.

3.6. Discussion of the data on ae mutant starches

These studies show that combined use of dry-cut sections in which starch is retained within cells, and KI/I_2 staining is a powerful method of observing structural heterogeneity in starch granules arising from mutations in biosynthesis. The observations on *ae* maize starch show that a discrete mutation involving the suppression of the activity of the starch branching enzyme IIb (SBEIIb) leads to significant heterogeneity of starch granule structure. Through use of a combination of spectroscopy and microscopy, it is possible to show that the blue- and pink-staining regions within the biphasic granules correspond to well-defined differences in chemical composition, type, degree and orientation of the ordered structures within the granules, and that there are ultrastructural differences, with a distinct transition region between the differentially stained parts of the granule. FEG-SEM, AFM and TEM can be used to probe the ultrastructure at the blocklet level within the granules. TEM studies using PATAG (periodic acid, thiosemicarbazide, silver)

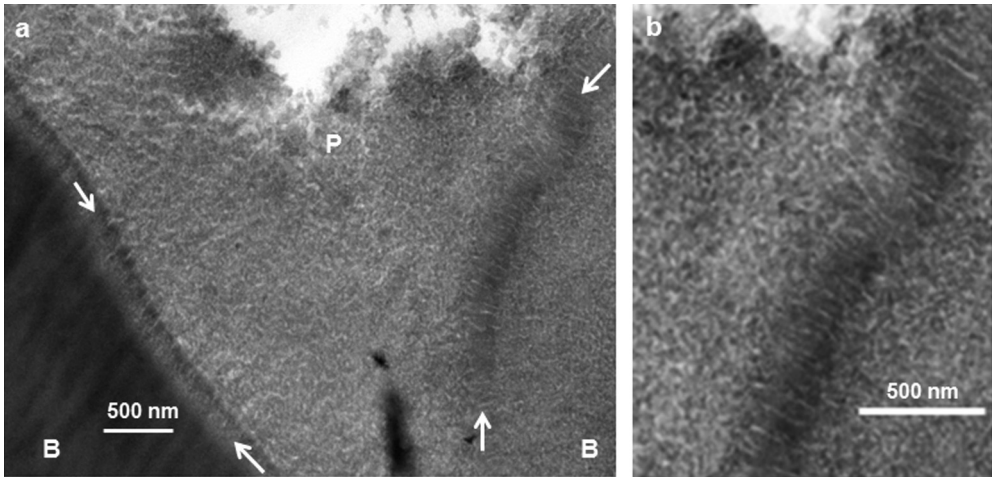

Fig. 8. TEM images of biphasic granules in inner endosperm cells at position T1 of *ae* kernels. (a) Image showing the ultrastructure within biphasic granules. The transition region of radially-elongated structures between the blue (B)- and pink (P)-staining regions is indicated by arrows. (b) Detail of the transition region showing the elongated structures. (For interpretation of the references to color in this figure legend, the reader is referred to the web version of this article.)

-staining (Gallant et al., 1997) offers the potential to visualise the location, orientation and size of the starch nanocrystals within the WT and in different regions within *ae* mutant starch granules.

The structures present in the blue- and pink-staining parts both differ from the structures present in the WT starch granules. Gallant and co-workers have investigated the enzymatic breakdown of starch granules isolated from high-amylose single (Planchot, Colonna, Gallant, & Bouchet, 1995) and double (Gérard, Colonna, Bouchet, & Planchot, 2001) maize mutants with the aim of elucidating the structural origins of the elevated resistance to α-amylase hydrolysis exhibited by these starches. SEM and TEM studies of α-amylase-degraded *ae* mutants were reported to show degraded structures inconsistent with the conventional 'onion ring' model of starch structure (Cameron & Donald, 1992; Daniels & Donald, 2003, 2004; Donald et al., 2001; Waigh et al., 1998; Waigh et al., 2000): rather the degraded granules showed a resistant outer layer of variable thickness present in the granules. It is possible that this is equivalent to the pink-staining region in which the structure is partially ordered (crystalline) but lacks the regular radial orientation present in the blue-staining regions of the granules. Comparative studies on a range of isolated high-amylose maize mutant starch granules (Jiang, Campbell, Blanco, & Jane, 2008; Li et al., 2008) suggests that the enzyme resistant (resistant starch) residues arise from crystalline amylose or intermediate material: the increased chain length of the amylosic chains in the crystals gives rise to the elevated melting temperatures of these crystals.

The use of *in situ* techniques to probe the internal structure of starch allows the distribution and level of heterogeneity to be mapped within the kernels. The present studies suggest that the highest level of heterogeneity is observed in the regions within the endosperm where the starch is first laid down and the distribution within the kernel suggests that the degree of heterogeneity is less in starch granules deposited later in grain development: the first cells containing starch are formed in the upper crown region of the kernel and further deposition moves progressively to cells in the basal region of the endosperm (Watson, 1987). The extreme variation in the structures of the granules suggests that, rather than the discrete mutation in an otherwise constant genetic background leading to a homogeneous starch granule structure, with simply a new ratio of 'amylose' to 'amylopectin', the mutation in fact appears to alter completely the physical structures of the starch granules, leading to a broad population of structural types. The major key feature appears to be a transition at various stages during the formation of the granule from ordered aligned structures to regions within the granule containing ordered, but unoriented structures, mainly indicated by progressive loss of radial alignment of the ordered structure. Such loss of radial alignment of ordered 'amylosic' structure in *ae* single mutant starch granules has also been suggested from a comparison of the differences in colours observed for iodine-stained isolated granules under bright field or polarising microscopy (Evans et al., 2003). This type of structural breakdown could most easily be considered to arise through the mutation in biosynthesis leading to the presence of defects during the self-assembly of the granules. These defects could accumulate to randomise progressively the physical state and arrangement of the crystalline structure within the granules. A possible mechanism by which such randomisation could occur would be through changes in the basic self-assembly of the platelet nanocrystals. Inhibition of SBEIIb activity might be expected to allow more amylosic chains to grow out of the faces of nanocrystals during biosynthesis, since the levels of branching would be reduced relative to the elongation, and cropping of the amylosic chains. Indeed the AFM and TEM images of the boundary region reveal fibrous structures at the surface of the blue regions indicating disruption of the radially-aligned structure. This could then disrupt nucleation of the next layer of platelet nanocrystals creating increasing levels of disorder during growth of the granule structure, through altering the orientation of subsequent crystals, and the chain length of the amylosic chains involved in these crystals. The FEG-SEM reveals that in the pink regions the size of the blocklets and their level of organisation are less regular. Previous Raman microscopy (Wellner et al., 2011) showed that these pink regions contained starch molecules with reduced levels of branching, compared to those in the blue regions, which were ordered (crystalline) but not radially-oriented. Such drastic disruption of the granule structure might lead to further loss of enzyme activity and increasing disorder, if an ordered surface is required for location and action of the biosynthetic enzymes. This explanation would not account for purely pink-staining granules, unless these arose due to the cutting or sectioning process missing the centre of these granules, and thus failing to reveal any blue-staining core region. Although the presence of defects could account for the subsequent disparity in granule structures it is necessary to explain how multiple ordered and aligned regions (Figs. 2–4) develop within single granules.

Granule structures containing multiple regions of radially-aligned, ordered (crystalline) structures ('compound granules') have been reported for high-amylose rice granules (Wei et al., 2010) and high-amylose maize (GEMS-0067) starch (Jiang, Horner,

et al., 2010). TEM studies (Jiang, Horner, et al., 2010) revealed the presence of a small number of amyloplasts containing two starch granules in WT maize, and demonstrated that the majority of amyloplasts in GEMS-0067 mutants contained two or more starch granules. Based on these observations it has been proposed that the 'compound' elongated structures isolated from GEMS-0067 and containing several radially-aligned, ordered structures, arise from the fusion of individual granules formed in the amyloplast (Jiang, Horner, et al., 2010). A similar explanation would account for the complex structures containing multiple blue-staining regions observed in the present studies on *ae* single maize mutants.

It is necessary to explain why the greatest level of heterogeneity arises in the regions where the starch is first laid down during development of the kernel. One suggestion is that as the kernel develops the granules in the outermost regions are younger, and the level of disorganisation is less, as there is less time for the cumulative effects of defects in biosynthesis to take effect. This seems the most likely explanation for the observed structures. An alternative hypothesis is that the starch laid down within the seed could be reused during development of the kernel: successive degradation and reassembly of the granules might be expected to enhance the effects of defects leading to increased levels of heterogeneity. However, there is at present no experimental evidence to suggest reuse of the starch within the *ae* kernel during development.

The progressive effects of defects on granule organisation could explain granule heterogeneity, but might not account for the marked and distinct changes in heterogeneity observed between adjacent cells or, what appears to be a reasonably well-defined transition near the periphery of the kernel (Fig. 3). The simplest explanation is that these sharp transitions at the outer extremities of the kernel reflect the time during development at which the granule size is insufficient for the pink regions to develop. A more complicated explanation could be that the transitions arise due to the effect of the mutation being moderated during development of the kernel, reducing the level of defects and the degree of disruption of the granule structure. Such an effect could be triggered by a change in environmental conditions, such as water content, during growth of the kernel, which might then explain the presence of a relatively sharp boundary region. In their discussion of the heterogeneity of high-amylose single and double mutants and its effect on enzymatic degradation, Gérard and co-workers (Gérard et al., 2001) cite studies (Denyer, Clarke, Hylton, Tatge, & Smith, 1996; Keeling, 1997; Singletary, Bansidr, & Keeling, 1997) indicating that spatial and temporal enzyme activity may indeed change during kernel development. Granule heterogeneity could be due to such temporal or spatial variation, arising from over expression of enzyme activity in the early stages of starch deposition, followed at a later time by induction of the severity of the mutation (Gérard et al., 2001). Alternatively it could arise from later compensation of the severity of the mutation during kernel development. To distinguish between these alternatives would require the identification and characterisation of the nature of any local variations in enzymatic activity during kernel development. There are comparative reported studies (Sidebottom, Kirkland, Strongitharm, & Jeffcoat, 1998) on different levels of bioactivity of starch branching enzymes in WT and high-amylose maize during kernel development, but understanding the development of starch granule architecture may require information on localised spatial and temporal variations, rather than averaged temporal variations for the whole seed.

4. Conclusions

A range of spectroscopic and microscopic methods has been used to identify and characterise structural heterogeneity in starch granule structure in *ae* maize mutants. The studies have been made *in situ* in mature kernels allowing the structural heterogeneity to be mapped in different parts of the kernel. These studies revealed that the highest level of structural heterogeneity appeared to occur in the starches deposited at the early stages of kernel development. The studies show that the single mutation at the *ae* loci leads to marked changes in granule structure resulting in a highly-diverse population of granules differing in chemical composition and physical chemical structure. This structural diversity will make it difficult to relate the 'average' chemical and physical chemical properties of extracted starch populations to the functional behaviour or nutritional properties of the isolated starch or flours. The distribution of structural heterogeneity within the kernel suggests that the overall level of structural heterogeneity increases during kernel development and is most pronounced in the granules deposited earliest in the development of the seeds. The different colours obtained through KI/I_2 staining and bright field microscopy allows different structural regions to be identified within individual granules. Subsequent use of a range of spectroscopic and microscopic methods allows these regions and nature of the boundary between the regions to be characterised. The studies reveal structural differences and transitions at the granule, cellular and tissue level. The methodology provides novel information on the changes resulting from development and growth of the kernel and could be used to investigate the effects of external environmental effects on growth and development, and thus starch structure. The study of starch structure within seeds provides novel information not obtainable from studies on isolated starches, and could be used to obtain information on the effects of isolation and processing on starch structure and function.

Acknowledgements

The research at IFR was funded through the core ISP grant to the Institute funded by the BBSRC. This study was enabled by BBSRC ISIS funding (BB/J004189/1), which led to further joint research between IFR and Zhejiang University. Research at Zhejiang University was supported by the Key Technologies R&D Programme of China (2012BAD29B04).

References

Blazek, J., & Gilbert, E. P. (2011). Applications of small-angle X-ray and neutron scattering techniques to the characterization of starch structure: A review. *Carbohydrate Polymers*, *85*, 281–293.

Blennow, A., Hansen, M., Schulz, A., Jorgensen, K., Donald, A. M., & Sanderson, J. (2003). The molecular deposition of transgenically modified starch in the starch granule as imaged by functional microscopy. *Journal of Structural Biology*, *143*, 229–241.

Cameron, R. E., & Donald, A. M. (1992). A small angle X-ray scattering study of the annealing and gelatinization of starch. *Polymer*, *33*, 2628–2636.

Campbell, M. R., Jane, J., Pollak, L., Blanco, M., & O'Brien, A. (2007). Registration of maize germplasm line GEMS-0067. *Journal of Plant Registrations*, *1*, 60–61.

Capron, I., Robert, P., Colonna, P., Brogly, M., & Planchot, V. (2007). Starch in rubbery and glassy states by FTIR spectroscopy. *Carbohydrate Polymers*, *68*, 249–259.

Chen, P., Yu, L., Chen, L., & Li, X. (2006). Morphology and microstructure of maize starches with different amylose/amylopectin content. *Starch-Stärke*, *56*, 611–615.

Daniels, D. R., & Donald, A. M. (2003). An improved model for analyzing the SAXS of starch granules. *Biopolymers*, *69*, 165–175.

Daniels, D. R., & Donald, A. M. (2004). Soft material characterization of the lamellar properties of starch: Smectic side-chain liquid-crystalline polymeric approach. *Macromolecules*, *37*, 1312–1318.

Denyer, K., Clarke, B., Hylton, C., Tatge, H., & Smith, A. M. (1996). The elongation of amylose and amylopectin chains in isolated starch granules. *Plant Journal*, *10*, 1135–1143.

Donald, A. M., Kato, K. L., Perry, P. A., & Waigh, T. A. (2001). Scattering studies of the internal structure of starch granules. *Starch-Stärke*, *53*, 504–512.

Evans, A., McNish, N., & Thompson, D. B. (2003). Polarization colors of lightly iodine-stained maize starches for amylose-extender and related genotypes in the W64A inbred line. *Starch-Stärke*, *55*, 250–257.

Gallant, D. J., Bouchet, B., & Baldwin, P. M. (1997). Microscopy of starch: Evidence of a new level of granule organization. *Carbohydrate Polymers*, *32*, 177–191.

Gérard, C., Colonna, P., Bouchet, D. J., & Planchot, V. (2001). A multi-stages biosynthetic pathway in starch granules revealed by the ultrastructure of maize mutant starches. *Journal of Cereal Science*, *34*, 61–71.

Hasjim, J., Srichuwong, S., Scott, M. P., & Jane, J. (2009). Kernel composition, starch structure, and enzyme digestibility of *opaque-2* maize and quality protein maize. *Journal of Agricultural and Food Chemistry*, *57*(5), 2049–2055.

Jiang, H., Campbell, M., Blanco, M., & Jane, J-L. (2008). Characterization of maize amylose-extender (*ae*) mutant starches: Part II. Structures and properties of starch residues remaining after enzymatic hydrolysis at boiling-water temperatures. *Carbohydrate Polymers*, *80*, 1–12.

Jiang, H., Horner, H. T., Pepper, T. M., Blanco, M., Campbell, M., & Jane, J. (2010). Formation of elongated starch granules in high-amylose maize. *Carbohydrate Polymers*, *80*, 534–539.

Jiang, H., Lio, J., Blanco, M., Campbell, M., & Lane, J. (2010). Resistant-starch formation in high-amylose maize starch during kernel development. *Journal of Agricultural and Food Chemistry*, *58*, 8043–8047.

Katz, F. R., Furesik, S. L., Tenbarge, F. L., Hauber, R. J., & Friedman, R. B. (1993). Behavior of starches derived from varieties of maize containing different genetic mutations – Effects of starch genotype on granular morphology. *Carbohydrate Polymers*, *21*, 133–136.

Keeling, P. L. (1997). Plant biotechnology: Technical barriers to starch improvement. In P. J. Frazier, P. Richmond, & A. M. Donald (Eds.), *Starch: Structure and functionality* (pp. 180–187). Cambridge, UK: The Royal Society of Chemistry.

Kirby, A. R. (2011). Atomic force microscopy of plant cell walls. In 'The Plant Cell Wall: Methods and Protocols', (ed: Popper ZA), Springer, NY, USA. *Methods in Molecular Biology*, *715*, 169–178.

Li, L., Jiang, H., Campbell, M., Blanco, M., & Jane, J. (2008). Characterization of maize amylose-extender (*ae*) mutant starches: Part I. Relationship between resistant starch contents and molecular structures. *Carbohydrate Polymers*, *74*(3), 396–404.

Liu, Y. L., Himmelsbach, D. S., & Barton, F. E. (2004). Two-dimensional Fourier transform Raman correlation spectroscopy determination of the glycosidic linkages in amylose and amylopectin. *Applied Spectroscopy*, *58*, 745–749.

Matsushima, R., Maekawa, M., Fujita, N., & Sakamoro, W. (2010). A rapid, direct observation method to isolate mutants with defects in starch grain morphology in rice. *Plant Cell Physiology*, *51*, 728–741.

Morris, V. J., Ridout, M. J., & Parker, M. L. (2005). AFM of starch: Hydration and image contrast. *Progress in Food Biopolymer Research*, *1*, 28–42.

Parker, M. L., Kirby, A. R., & Morris, V. J. (2008). In situ Imaging of pea starch in seeds. *Food Biophysics*, *3*, 66–76.

Pérez, S., & Bertoft, E. (2010). The molecular structures of starch components and their contribution to the architecture of starch granules: A comprehensive review. *Starch-Stärke*, *62*, 389–420.

Planchot, V., Colonna, P., Gallant, D. J., & Bouchet, B. (1995). Extensive degradation of native starch granules by α-amylase from *Aspergillus fumigatus*. *Journal of Cereal Science*, *21*, 163–171.

Ridout, M. J., Gunning, A. P., Wilson, R. H., Parker, M. L., & Morris, V. J. (2002). Using AFM to image the internal structure of starch granules. *Carbohydrate Polymers*, *50*, 123–132.

Ridout, M. J., Parker, M. L., Hedley, C. L., Bogracheva, T. Y., & Morris, V. J. (2004). Atomic force microscopy of pea starch: Origins of image contrast. *Biomacromolecules*, *5*, 1519–1527.

Seckinger, H. L., & Wolf, M. J. (1966). Polarization colors of maize starches varying in amylose and genetic background. *Starch-Stärke*, *18*, 2–5.

Sidebottom, C., Kirkland, M., Strongitharm, B., & Jeffcoat, R. (1998). Characterization of the differences of starch branching enzyme activities in normal and low-amylopectin maize during kernel development. *Journal of Cereal Science*, *27*, 279–287.

Singletary, G. W., Bansidr, R., & Keeling, P. (1997). Influence of gene dosage on carbohydrate synthesis and enzymatic activities in endosperm of starch-deficient mutant of maize. *Plant Physiology*, *113*, 293–304.

van de Velde, F., van Riel, J., & Tromp, R. H. (2002). Visualisation of starch granule morphologies using confocal laser scanning microscopy (CSLM). *Journal of Science Food and Agriculture*, *82*, 1528–1536.

vanSoest, J. J. G., Tournois, H., deWit, D., & Vliegenthart, J. F. G. (1995). Short-range structure in (partially) crystalline potato starch determined with attenuated total reflectance Fourier-transform IR spectroscopy. *Carbohydrate Research*, *279*, 201–214.

Waigh, T. A., Perry, P. A., Rickel, C., Gidley, M. J., & Donald, A. M. (1998). Chiral side-chain liquid-crystalline properties of starch. *Macromolecules*, *31*, 7980–7984.

Waigh, T. A., Kato, K. L., Donald, A. M., Gidley, M. J., Clarke, C. J., & Rickel, C. (2000). Side-chain liquid-crystalline model for starch. *Starch-Stärke*, *52*, 450–460.

Watson, S. A. (1987). Structure and composition. In S. A. Watson, & P. E. Ramstad (Eds.), *Corn: Chemistry and technology* (2nd ed., pp. 53–82). St-Paul, MN, USA: American Association of Cereal Chemists.

Wei, C., Qin, F., Zhu, L., Zhou, W., Chen, Y., Wang, Y., et al. (2010). Microstructure and ultrastructure of high-amylose rice resistant starch granules modified by antisense RNA inhibition of starch branching enzyme. *Journal ofAgricultural and Food Chemistry*, *58*, 1224–1232.

Wellner, N., Georget, D. M. R., Parker, M. L., & Morris, V. J. (2011). In situ Raman microscopy of starch granule structures in wild type and ae mutant maize kernels. *Starch-Stärke*, *63*, 128–138.

Zhu, L-J., Dogan, H., Gajula, H., Gu, M-H., Liu, Q-Q., & Shi, Y-C. (2012). Study of the kernel structure of high-amylose and wild-type rice by X-ray microtomography and SEM. *Journal of Cereal Science*, *55*, 1–5.